

Phase Separation of Active Colloidal Suspension via Quorum Sensing

Francis Jose,* Shalabh K. Anand,† and Sunil P. Singh‡

*Department of Physics,
Indian Institute Of Science Education and Research,
Bhopal 462 066, Madhya Pradesh, India*

(Dated: June 30, 2022)

We investigate the dynamics of a dilute suspension of active colloidal system whose self-propulsion speed is modulated according to the local density using rules adherent to quorum sensing. A coarse-grained Brownian dynamics simulations approach is employed to study the dynamics of active colloidal system. The transition from homogeneous gaseous-state to a liquid-like cluster and the long-range ordered crystal-like cluster is characterized through their size and structure analysis. We show that how the prospective choice of concentration dependent motility of colloidal particles affects their collective dynamics and leads to living crystal in the system at very low packing fraction $\phi = 0.15$ for very high self-propulsion speed. The transition boundary of these phases are identified via local-order and global bond order parameters, bond-correlation, and swim pressure of the system. In addition, we have shown that the qualitative behavior of effective diffusion coefficient and swim pressure exhibit similar characteristic feature.

I. INTRODUCTION

A collection of self-propelled units constitutes an out-of-equilibrium system, which harvest ambient energy from the environment to execute persistent motion [1–3]. They exhibit remarkably complex collective dynamics which is absent in its passive counterpart, such as self-organization at low density [4–11], flocking [12, 13], swarming [14], vortex-formation [15], formation of linear chains [16], anomalously large density fluctuations[17], non-monotonic behavior of active pressure [18, 19], etc. The phase separation of such system has been rigorously explored by synthetically designed objects in lab where they can manipulate dynamical structures by means of light control motion of active colloid[15, 20, 21], diffusio-phoretic motion, or chemical gradients of various species, etc [21–27].

The recent investigations in the area of active colloids are mainly categorised in two themes, one is ordering due to alignment interactions [17, 28–33], and other one is motility induced phase separation (MIPS) [17, 33–44]. The alignment interaction breaks the symmetry of system, and exhibits ordering in the velocity field that leads to the structural organisation [5, 28, 45–51]. The later case, the MIPS, is a consequence of steric and self-propulsion forces [52], here a dense aggregate coexist together with a low density gaseous phase[17, 33–43] at packing fractions below the liquid-gas transition point ($\phi \approx 0.4$) [17].

The coordinated motion in many biological systems is consequence of complex communication pathways among distinct individual units as the few bacterial colonies produce extra-cellular molecular enzymes or anti-bacterial

agents [53, 54]. In another example, bio-luminescent bacteria *Aliivibrio fischeri* [55] produces luminescence after sensing their population density beyond a certain threshold value. The communications among them is termed as ‘quorum sensing’, as it regulates their ability for biochemical processes namely for the growth of local population density and regulation of gene expression [55, 56], communication among cells [57], their motility[56, 57], etc. The ability of self-regulation of the motility have been adopted in simpler models for the motile rod like colloids in simulations resulting a rich dynamical phase diagram [58, 59]. The introduction of an analytic function to regulate motility imparting a local density dependence serves similar purpose in numerical calculations [60]. The question arises here that how the ability of self-regulation of motility affects the spontaneously emerged phase separation of active colloidal systems? In theoretical models, two types of self-propulsion mechanisms have been proposed for the active matter systems, one is the ‘run and tumble’ model [61], where the direction of motion abruptly changes this model has been employed for various bacterial species [62–64]. In the other description, named as Active Brownian particle(ABP) model, the direction of motion continuously varies and it is dictated by the rotational diffusion coefficient [33, 58, 65–72].

Here, we perform molecular dynamics simulations of a dilute suspension of ABPs. To regulate their speed in a very simple manner, the self-propulsion speed is considered as a linearly decreasing function of the local density. Our simulations reveal that the density regulated motility enhances the cluster formation and results in living crystals at a packing fraction as low as $\phi \approx 0.15$. The largest cluster size and its distribution reveals a dense phase surrounding with the low density phase beyond a critical density. The local and global order parameter defined from the the angle between nearest neighbors, Θ , and a bond orientation parameter Ψ_6 and C_{q_6} signifies the hexatic ordering at large Péclet numbers. The dynamics of colloids are quantified in terms of

* fjose@iiserb.ac.in

† skanand@iiserb.ac.in

‡ spsingh@iiserb.ac.in

the mean-squared-displacement (MSD), it displays sub-diffusive behavior in the short-time with a plateau in the intermediate time range. The effective diffusion coefficient and the swim pressure in the phase separated states display a cross over from the parabolic increase to a power law with an exponent 3/2 on Péclet number. In addition to that, the stability of the cluster is recognised in terms of the large repulsive and self-propulsion forces at the cluster boundaries.

We have organised article as follows: Section II elaborates the simulation approach, all the results are presented in section III and they are summarised in section IV.

II. SIMULATION MODEL

We model a collection of self-propelled polar units in two dimensions driven by locally variable force. These units interact with each other via repulsive-shifted Lennard Jones (LJ) potential given as,

$$U_{LJ}(r_{ij}) = \begin{cases} 4\epsilon \left[\left(\frac{\sigma}{r_{ij}}\right)^{12} - \left(\frac{\sigma}{r_{ij}}\right)^6 \right] + \epsilon, & r_{ij} \leq 2^{1/6}\sigma \\ 0, & r_{ij} > 2^{1/6}\sigma. \end{cases} \quad (1)$$

Here, i and j are particle index, $r_{ij} = |\mathbf{r}_i - \mathbf{r}_j|$ is the distance between the pair, ϵ is the LJ energy, and σ is the diameter of the disk. These particles are considered as polar units and its orientation vector is given as $\hat{\mathbf{e}}$.

The equation of motion of a particle and its orientation vector is governed by the over-damped Langevin equation,

$$\begin{aligned} \dot{\mathbf{r}}_i &= \frac{1}{\gamma} \left[\sum_{j=1}^{N_m} (-\nabla_i U_{LJ}(\mathbf{r}_{ij})) + F'_{a,i} \hat{\mathbf{e}}_i + \mathbf{F}_i^R \right], \\ \dot{\theta}_i &= F_i^\theta. \end{aligned} \quad (2)$$

Here γ is the drag coefficient, F_i^R is the thermal noise with zero mean, $F'_{a,i}$ is magnitude of the active force, and its direction is given by the orientation unit vector $\hat{\mathbf{e}}_i = (\cos \theta_i, \sin \theta_i)$. The direction of polar vector $\hat{\mathbf{e}}$ obeys the rotational diffusion with an angle θ_i , measured from the x-axis. The friction coefficient and the thermal noise are coupled via fluctuation-dissipation relation, $\langle F_{i\alpha}^R(t) F_{j\beta}^R(t') \rangle = 2\gamma \delta_{\alpha,\beta} \delta_{ij} k_B T \delta(t-t')$. Similarly, F_i^θ is a random torque on a particle, and the relation of random torque with rotational diffusion is given as $\langle F_i^\theta(t) F_j^\theta(t') \rangle = 2D_r \delta(t-t') \delta_{ij}$. Here, $D_t = \frac{k_B T}{\gamma}$ and $D_r = \frac{3D_t}{\sigma^2}$ are the translational and rotational diffusion constants, respectively.

We take into account the effect of local environment on the motility in a very approximate manner. For the simplicity, F_a here is assumed to be a linear function of its nearest neighbors in a cut-off distance of $R_c \leq 1.3$. Thus the active force is linearly diminishing with the growth

of local population as,

$$F'_{a,i} = \begin{cases} F_{a,i}, & n < 2, \\ \beta F_{a,i} \left(1 - \frac{\phi_i}{\phi_m}\right), & 2 \leq n \leq 6. \end{cases} \quad (3)$$

Here, n stands for the number of nearest neighbor to particle i , $F_{a,i}$ is the active force on an isolated particle that is modified to $F'_{a,i}$ in the presence of neighbors within a cut-off distance of $R_c = 1.3\sigma$. The prefactor $\beta \approx 1.8$ is chosen so that the function is calibrated to be linearly decreasing from $F'_{a,i} = F_{a,i}$ at $n = 2$ to $F'_{a,i} = 0$ at $n = 6$. Once center of a neighboring particles cross the cut-off, the particles are assumed to be completely inside the screening area. The apparent local area fraction in the circle of radius R_c with particle i at the center is approximated as $\phi_i = \alpha(\pi\frac{\sigma^2}{2} + n\mathcal{A})$ here $\alpha = (\pi R_c^2)^{-1}$, and $\mathcal{A} \approx 0.6531\sigma^2$ is the approximate area of the disk located within the the cut-off distance R_c . The maximum packing fraction within the cut-off radius is given by, $\phi_m = \alpha(\pi\frac{\sigma^2}{2} + 6\mathcal{A})$.

All the parameters presented in this manuscript are in dimensionless form, where length is scaled by σ (diameter), energy is in unit of $k_B T$ (thermal energy), and time is in unit of $\tau = \sigma^2/D_t$. The Brownian dynamics method is employed with a time step of $10^{-4}\tau$ to $10^{-5}\tau$ and rotational diffusion $D_r = 3D_t/\sigma^2$. The simulation box is taken to be a square and periodic in each direction. All the results are quantified in parameter landscape of packing fraction $\Phi = \frac{\pi\sigma^2 N}{4L^2}$ and dimensionless Péclet number $Pe = \frac{F_a \sigma}{k_B T}$ in equivalence of self-propulsion speed. The number of particles are taken $N = 1225$, which is kept constant for all the parameters. The simulation box is varied to achieve the packing fractions 0.05 to 0.3, and Pe is varied in the range of 0 to 250. The statistics for each data set is generated by averaging over 20 independent sets.

III. RESULTS

A collection of self-propelled hard-colloids yields a very rich collective phase behavior [1, 2, 17, 33]. The presence of short-range physical or chemical attraction among them further aids noticeable influence on the local inhomogeneity, separation of chemical mixtures and re-entrant phase behavior of active colloids [11, 73]. A density dependent motility enhances the richness of the phase diagram of such systems. Here, we reveal the role of density dependent self-propulsion on the aggregation of repulsive self-propelled system.

A. Phase Separation

A few snapshots of emergent structures at various activity strengths are displayed in Fig. 1-a, b, c, and d.

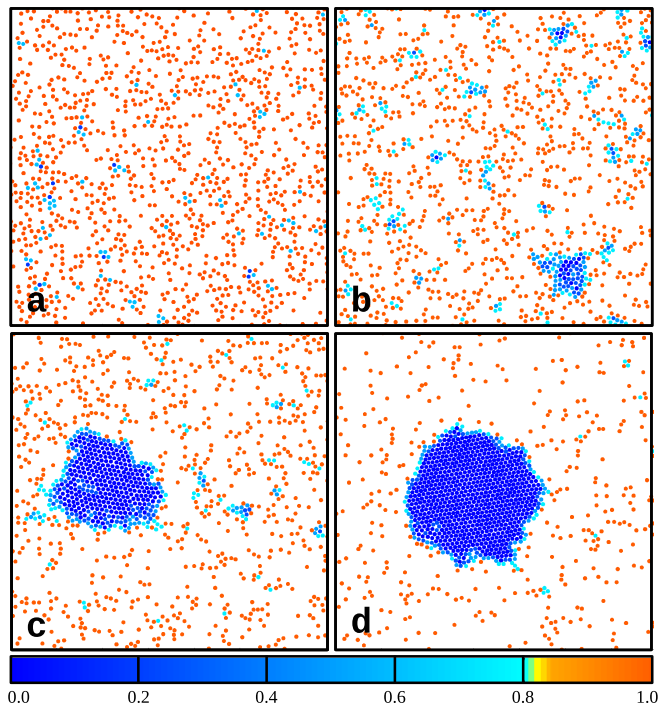


FIG. 1. A set of snapshots of the system at $\Phi = 0.20$ at a) $Pe = 5$, b) $Pe = 50$, c) $Pe = 60$, and d) $Pe = 200$. The particles are color coded according to their fraction of their self-propulsion force with the unperturbed active force. The gradient of color shows the speed of the particles from fast motion (red) to slow motion (blue).

In the limit of low Péclet number, a group of smaller clusters are formed, these clusters grow in size at the intermediate $Pe < 60$, exhibiting a liquid-like characteristics (See Fig. 1-a and b). Our simulations show a dense aggregation of self-propelled colloids with a long-range structure even at a very small packing fraction, $\Phi \approx 0.15$, as Fig. 1-c and d illustrates. The bigger aggregates find frequent collisions with freely moving individual active particles at higher swimming speed, i.e., $Pe \gg 1$. After collision with cluster their speed dramatically slows down, comparatively slow rotational diffusivity causes them to be part of the aggregates until their orientation changes. Consequently, size of the aggregate exhibit instantaneously a sharp growth in the size.

These snapshots clearly reveal that for smaller values of $Pe < 1$, system remains in a gaseous-like phase with a few very small dynamic aggregates. In this regime, thermal fluctuations overpower the active force and maintains the homogeneity in the space, analogous to the passive system. The size of these aggregates grows with increasing Pe . In the intermediate regime nearly at $10 < Pe < 60$, the smaller clusters are formed with short life time, which breaks and forms throughout the system for $\Phi = 0.20$. The size of the largest cluster grows with Pe and eventually becomes of the order of the system size in the asymptotic limit of $Pe > 50$ as evident from Fig. 1-c ($Pe = 60$) and d ($Pe = 200$).

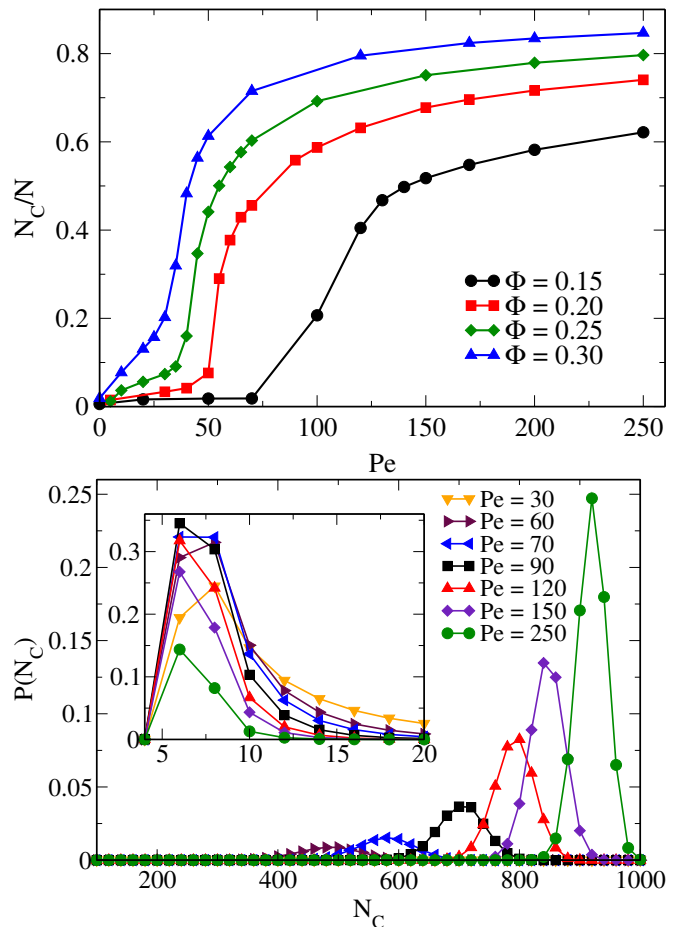


FIG. 2. a) The normalized average cluster size N_C/N as a function of Pe for various packing fractions $\Phi = 0.15, 0.2, 0.25,$ and 0.3 . b) The distribution of the cluster size $P(N_C)$ for various $Pe = 30, 60, 70, 120, 150,$ and 200 . Inset shows distribution of smaller clusters which lie in the range of 0 to 20 at $\Phi = 0.20$. Note this is not shown in the main plot.

The phase separation even at low density is a consequence of slowing down of the colloid after the collision at the interface and it goes inside a cluster as it finds more neighbors. The multi-body collision grows with Pe , hence the probability of finding many particles together in a small neighborhood increases, which results instantaneous slow down of the propulsion speed as proposed in the activity screening scheme of Eq. 3. This effect is illustrated in the snapshots by colors where blue is for the slow moving particles as opposed to fast moving from the red (see color bar in Fig.1). It is evident from the snapshots that deep inside a cluster or at interface, particle speed is relatively slower than the outside one. Therefore the slow motion of a cluster encounters frequent collision with the fast moving particles leading to slow them as well. As a consequence, growth of the cluster increases with speed of the swimmers.

The inhomogeneity in the system grows with Péclet number and this can be quantified through the size of

aggregate, specifically the largest one (N_C) and the size distribution of aggregates. This will be able to provide a measure for the transition from an isotropic phase to a bimodal phase mixed with liquid-like aggregates with gaseous-phase. The size of largest cluster is computed assuming that the particles which lie within a chosen threshold distance (1.3σ) with each other are connected and they are accounted as a part of a cluster. Fig. 2-a displays the average size of the largest cluster N_C as a function of Pe for packing fractions $\Phi = 0.15, 0.2, 0.25$ and 0.3 . The average size of cluster, beyond the critical value $Pe > Pe_c$, becomes quickly of the order of the system size. For $Pe \gg Pe_c$, its growth becomes very slow. Although, the largest cluster diffuses and its shape continuously fluctuates over the time, but the average size of cluster is nearly stable. In addition, the transition for denser system occurs at smaller critical Pe , which is effect of larger many-body collision at higher Φ , as a result aggregation of small clusters within the system occurs at smaller Pe .

In the phase separated state, the coexistence of larger clusters with gaseous state can be qualitatively accessed from the distribution of its size. For this we compute the distribution $P(N_C)$ as presented in Fig. 2-b. The distribution illustrates a single peak for the smaller cluster size for all Pe . The height of peak diminishes with Pe , which can be seen in the inset of Fig. 2-b. For the better visualisation distribution is split into two parts, smaller clusters are in the inset and larger one is in the main plot of Fig. 2-b. The peaks for large cluster size appears nearly at $Pe \geq 60$ and it shifts towards larger size with very pronounced height. The presence of bimodal peaks in the distribution is a signature feature indicating the coexistence of two phases.

B. Structure of Cluster

Evidently, long-range ordering with a hexagonal crystalline structure is prevalent in the largest aggregate after phase separation. To quantify the internal structure and its ordering in 2D, we analyse an angle Θ between two successive vectors connecting the six nearest neighbors of each particle. The definition of Θ , as exemplary, is illustrated in Fig. 3-a. This is defined in a way that for a perfect hexagonal structure it contains sharp peaks in the distribution, $P(\Theta)$, at the values of $\Theta = 60, 120, 180, 240$ and 300 and peak at 0 or 360 are ignored. For $Pe < 60$, the distribution is flat exhibiting no peaks, thereby suggesting a homogeneous phase without any long-range ordering. As anticipated, sharp peaks in the distribution of Θ spontaneously appear in Fig. 3-a for a larger $Pe \geq 60$. Besides the increase in the height of the peaks, their widths are localised to the aforementioned angles with increase in Pe .

The distribution of Θ reveals a hexagonal ordering in the regime of large Pe . To further corroborate our claim of the hexagonal phase in the largest cluster, we analyse

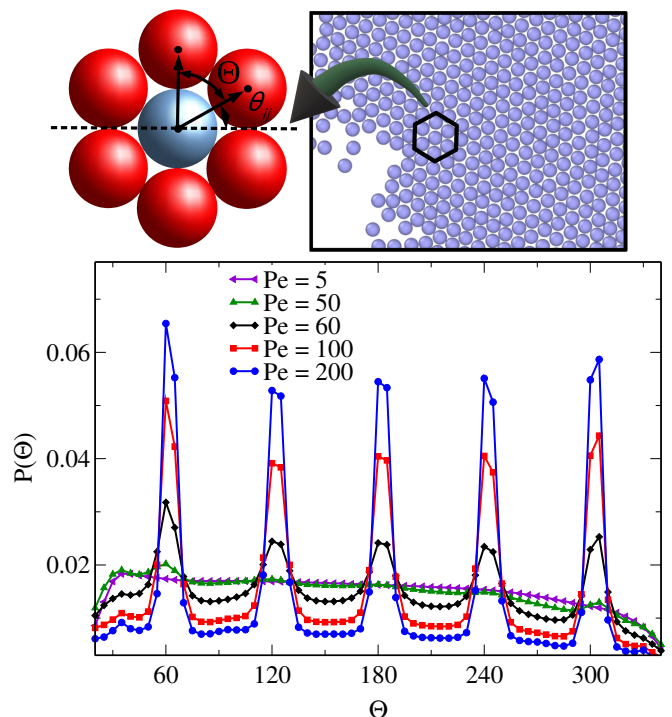


FIG. 3. a) The definition of different angles used in analysis of the ordered phase; Θ for the angular distribution and θ_{ij} for the calculation of order parameter, q_6 . b) The distribution of Θ between vectors connecting centres of the particles to its six nearest neighbours at $\Phi = 0.20$.

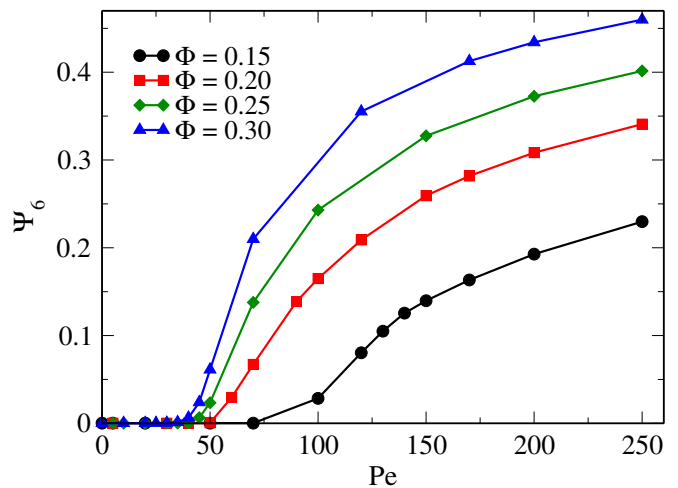


FIG. 4. The average value of Ψ_6 as a function Péclet number for various Φ . The value of Ψ_6 shows a steady increase with Pe after the critical point for phase separation. The value of Ψ_6 increases with Φ as well.

the bond orientational order parameter proposed in the literature [65, 74–77],

$$q_6(i) = \frac{1}{6} \sum_{j \in \mathcal{N}(i)} e^{i6\theta_{ij}}, \quad (4)$$

where $\mathcal{N}(i)$ runs over six nearest neighbors of i^{th} particle and θ_{ij} is the bond angle between a pair ij around an arbitrary axis (see Fig. 3-a). From the local parameter, we estimate a global order parameter [65],

$$\Psi_6 = \left\langle \left| \frac{1}{N} \sum_{i=1}^N q_6(i) \right|^2 \right\rangle. \quad (5)$$

The global order parameter Ψ_6 , lies in the range of $[0, 1]$, where 0 represents for the isotropic phase of the system and 1 is for the perfect crystalline phase [65, 74–77]. The order parameter Ψ_6 is zero in the limit of small Péclet number $Pe < 60$, and for $Pe > 60$ at $\phi = 0.15$, it becomes non-zero with a sharp rise in its value as Fig.4-a illustrates. The non-zero values of Ψ_6 reveal the presence of long-range ordering within the structure. In the case of denser suspensions, the phase transition appears for relatively smaller Péclet number. Analogous to Ψ_6 , we can employ another parameter, correlation of the q_6 parameter, C_{q_6} , which shows bi-modal peaks in the phase separated states (see Fig. SI.3).

C. Force Distribution

The local density $\rho(R)$ of the cluster from its centre-of-mass is estimated and displayed in Fig. 5-a. The density within the cluster remains constant near the centre while it falls sharply towards the edges of the cluster and hence provides an estimate of the average radius of the cluster. The decay of density near the edges falls sharply for higher Pe , suggesting relatively small fluctuations near boundaries. The physical forces responsible for a stable cluster in the crystalline state against the entropic forces are analysed here. The total force on the largest cluster w.r.t. its centre of mass (R_{CM}) assuming that the cluster is spherically symmetric is presented here. The magnitude of total repulsive and active forces on the largest cluster are displayed in Fig. 5-(b). The magnitude of repulsive LJ force deep inside the cluster is constant and it slowly dies towards the effective boundary. The plateau value of the repulsive force in the bulk grows with Pe as a consequence of much denser structure at high Pe as shown in Fig. 5-a. The density of particles in outer region is smaller, hence, in this range the magnitude of repulsive force from the nearest interactions yields the smaller values (See Fig.5-a).

Surprisingly, for larger $Pe \gg Pe_c$, the LJ force near the boundary develops a peak for $Pe > 60$ near $|R - R_{CM}| \approx 17$. The height of peak grows in a very pronounced way with Pe . The peak in the repulsive force can be corroborated by the magnitude of the self-propulsive force on the surface, this is shown on the same plot with shaded symbols (see Fig. 5-b). Evidently, the self-propulsion force reflects a maximum near the surface and it dies towards the boundary and deep inside the cluster. This is along the line of our assumption in Eq. 3

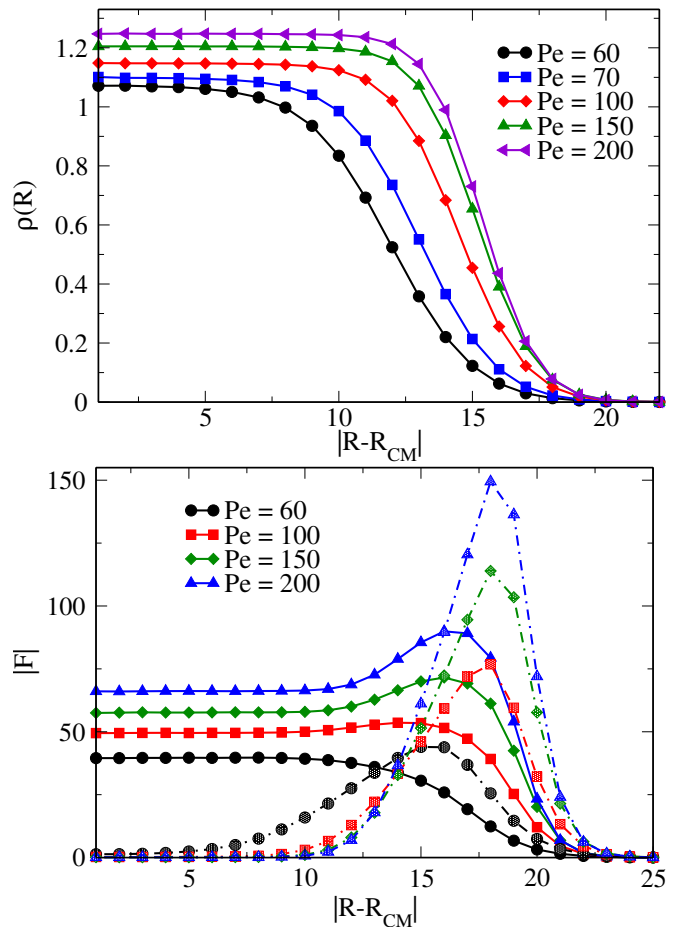


FIG. 5. a) The spatial variation of density of the cluster as a function of radial distance $|R - R_{cm}|$ from its centre of mass at $\Phi = 0.20$. b) The magnitude of average repulsive force F_{LJ} (filled symbols) and active force F'_a (shaded symbols) on the largest cluster as a function of distance from the centre-of-mass $|R - R_{cm}|$ of the cluster for various Péclet numbers as shown in the plot at $\Phi = 0.20$.

that at the higher density self-propulsion force remains close to zero. The particles at the edge of the cluster are having lesser number of neighbors which makes activity higher on the edges accordingly and the propulsion speed deep inside the cluster is smaller.

The magnitude of large active force on the surface causing the inward pressure from the surface molecules results in a large repulsion on the surface. This repulsion and magnitude of the active forces grow with $Pe \gg Pe_c$. The internal pressure balanced from the active force on the surface results in a stable active crystalline phase which emerges even at very small densities. For smaller $Pe < 50$, the difference in the average force F_{LJ} and F'_a is small, because of which, the entropic forces dominate over the effective attractive force. Hence, fluctuations at the boundaries are dominant over the inward repulsion along the boundary prior to the critical density. In summary, the collision due to active force results

a peak in repulsive force and slow rotational diffusion of polar molecules results large active inward pressure, which holds the stable cluster across the system.

D. Dynamics of cluster

The dynamical behavior of the colloids in the aggregates can be accessed via its mean-square-displacement (MSD). However, this is a non-trivial task in terms of computation since the cluster is not in a frozen-state although it has long-range crystalline-structure. A colloid inside the cluster is highly mobile at larger time-scales. In order to compute the MSD of a molecule, we choose only those molecules of the largest aggregates close to centre of the cluster so they do not leave the cluster in the estimated time-scale. As expected, at short time-scales, it has sub-diffusive behavior due to the constraint to the motion in the presence of neighbors in the close proximity (see Fig.6-a). Furthermore, at the intermediate time scales, as the self-propulsion is mostly being suppressed and the particles are caged in the aggregates, the MSD shows a plateau which further suggests the suppression of any kind of motion at this scale. More importantly, the width of the plateau regime becomes prominent at higher Pe , as it continually extends to the larger time-scales as Fig. 6 reveals for $Pe = 70, 90, 150, 200,$ and 250 . At larger time scales, the particles diffuse faster and it may drift away from the center, hence the MSD attains super-diffusive behavior. This causes the enhanced dynamics of the colloids as evident for $Pe = 70$ curve at latter timescales ($t > 0.1$). A dashed line shows the super-diffusive behavior with $\langle \Delta r^2(t) \rangle \sim t^{3/2}$ with an exponent $3/2$. The super-diffusive regime for larger Pe will also appear for the larger time-scales, although the exponent may not be the same.

In addition to the local short time dynamics of colloids, we further estimate the average characteristic feature of the colloids from the effective diffusion coefficient. Here, we calculate the MSD of the colloids averaged over all the particles in the system. The MSD of the active colloids exhibits sub-diffusive (short time), super-diffusive (intermediate time) followed by the diffusive (long time) regime for the phase separated states (See Fig. SI-4). The effective diffusion coefficient obtained from the diffusive regime is plotted as a function of Pe in Fig.6-b. In the homogeneous phase, effective diffusion coefficient increases quadratically. Interestingly, for the large Pe the increase in D_τ is less than the quadratic dependence, where it grows with a power-law behavior with an exponent $3/2$ for $\Phi \geq 0.15$. Thus, the translational diffusion coefficient exhibits a cross-over from Pe^2 (quadratic) in homogeneous to $Pe^{3/2}$ behavior in the phase separated state. The inset of the curve shows the behavior of the normalized D_τ/D_τ^0 , where $D_\tau^0 = D_t + 3Pe^2/2$ is the effective diffusion coefficient for ideal active particles at same Pe . As expected from the effective diffusion coefficient, the dynamics of particle substantially slows down with

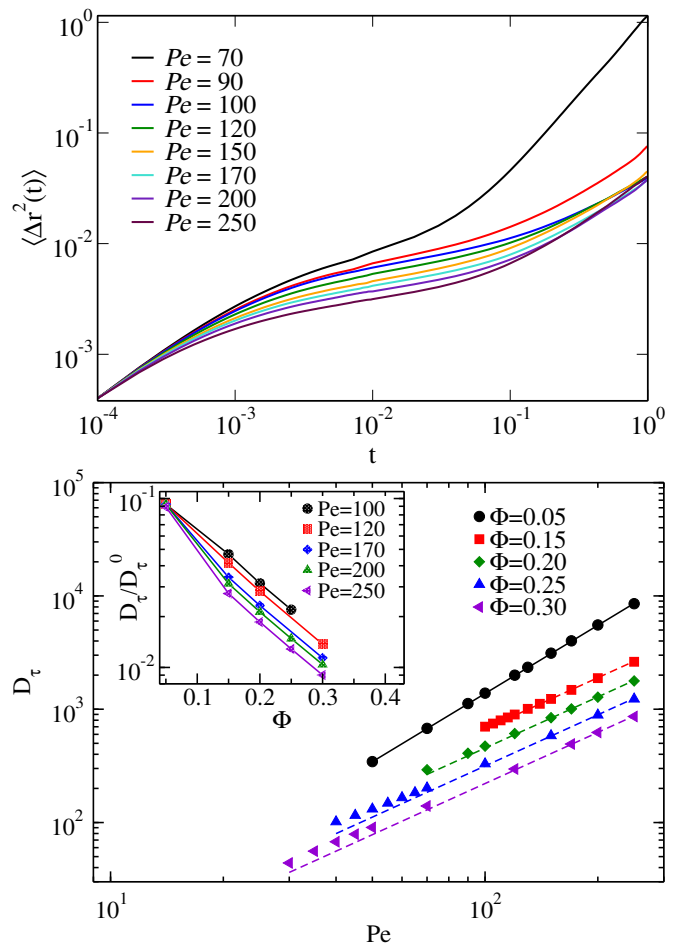


FIG. 6. a) The mean-square-displacement (MSD) of particles deep inside the clustered region for different Pe . The dashed line shows the super-diffusive behavior as $t^{3/2}$. b) The effective diffusion coefficient as function of Péclet number for various $\phi = 0.05, 0.15, 0.2, 0.25$ and 0.3 . The solid line shows power law behavior, $D_\tau \approx Pe^2$, and dashed lines as $D_\tau \approx Pe^{3/2}$. The inset shows normalized D_τ/D_τ^0 with Φ for various Pe as function Φ . Here, D_τ^0 is the effective diffusion coefficient [18, 19] of the ideal non-interacting active particles at same Pe .

the we clearly see D_τ decreases with packing for Pe [18].

E. Swim Pressure

The pressure within MIPS can be used to identify phase boundaries as it exhibits a non-monotonic behavior on density with sharp jump near the transition point [18, 37]. The total pressure has contributions from the thermal fluctuations, the interaction force, and the active force which is termed as swim pressure. The pressure per particle can be expressed as $p = p_0 + p_a + p_{in}$, where $p_0 = k_B T/A$ is the ideal gas pressure in 2D, p_a is the swim pressure, and p_{in} is the standard virial pressure

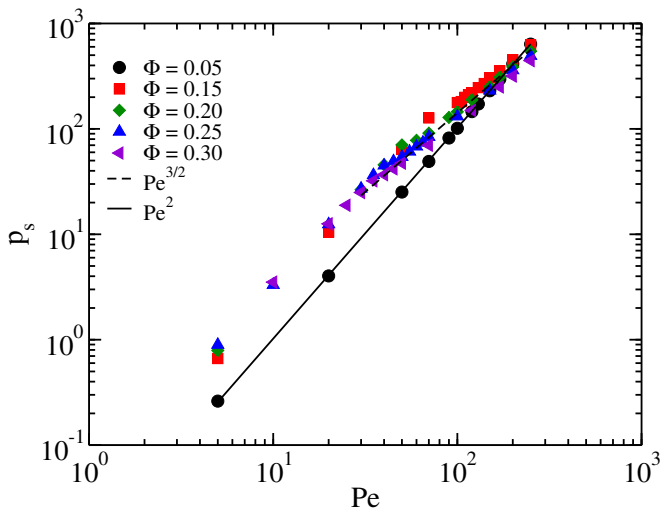


FIG. 7. The swim pressure p_s plotted as a function of Pe for different ϕ . The behavior of in swim pressure with solid line Pe^2 and dashed line $Pe^{3/2}$.

term due to inter-particle interactions. They are given as,

$$\begin{aligned}
 p_a &= \frac{\gamma}{2AN} \sum_i^N \langle F'_{a,i} \hat{\mathbf{e}}_i \cdot \mathbf{r}_i \rangle \\
 p_{in} &= \frac{1}{4AN} \sum_{j,i}^N \langle \mathbf{F}_{ij} \cdot (\mathbf{r}_i - \mathbf{r}_j) \rangle.
 \end{aligned}
 \tag{6}$$

The above expression for the total pressure $p(\Phi)$ defines an equation of state of ABPs without confinement. In the dilute limit, inter-molecular interaction diminishes and the swim pressure in a 2D system is given as $p_{id}A = k_B T(1 + 3Pe^2/2)$ at a given temperature [18, 19]. The swim pressure increases quadratically with activity for small Pe or Φ as Fig. 7. At higher density the total pressure p is dominated by the swim pressure, therefore we analyse characteristics of swim pressure. Fig. 7 illustrates the swim pressure in the system plotted against Pe . The swim pressure grows quadratically in the limit of small Pe , until a phase separation occurs within the system. It is denoted by the change in the behavior of power-law near the critical Pe for the phase separation corresponding to $\Phi \geq 0.15$. This behavior is in contrast to the trend shown by $\Phi = 0.05$, where there is no apparent phase separation and swim pressure increases with quadratically as $p_s \sim Pe^2$. For Pe greater than the critical Péclet number, the swim pressure grows with power law behavior as $p_s \sim Pe^{3/2}$. The change in the behavior of the swim pressure in the phase separated state is a consequence of large-number fluctuations in the active systems (See Fig. SI-2 for anomalous density fluctuations). In the limit of large Pe , the power-law exponent for the swim pressure is same as for the effective diffusion coefficient as suggested in Ref. [18].

IV. SUMMARY

We have presented the Langevin dynamics simulations of polar active colloids whose motility is a dynamic quantity varying with its local density. At higher Péclet number, the system phase separates into cluster of living crystals with a hexagonal ordered phase even at a much smaller packing fraction ($\Phi = 0.15$) than the previously reported results [11, 34, 65]. We have shown that a homogeneous phase spontaneously separates into the ordered crystalline aggregate, which has been quantified in term of the largest aggregate and its size distribution. The transition point is identified by employing a global order parameter Ψ_6 and correlation function C_{q_6} , which clearly demonstrates the hexatic ordering inside the cluster.

Furthermore, we have shown the microscopic origin behind the aggregation in active system in terms of the repulsive and active force. The large inward active force on the surface causing the inward pressure on the surface molecules results in a large repulsion on the surface. The internal pressure balances from the large active force on the surface resulting an active crystalline phase which emerges even at very small densities. The profile of the repulsive forces certifies our claim with uniform force inside the cluster, and sharp increase near boundary with similar behavior for the magnitude of active force near the surface. The slow rotational diffusion of polar molecules results in a large inward active pressure which is responsible for rendering the cluster stable across the time-series without breaking, similar to the surface tension which retains boundary in liquids. The presented result is not unique for the adopted linear model proposed in Eq.3, we have also verified the results for an exponentially decaying self-propulsion force. It also shows the same qualitative behavior as few results presented in the Supplementary text see Fig. SI-6, and 7. The dynamics of active particles in the cluster exhibits sub-diffusive behavior at short time due to caging from its neighbors. In addition, our simulations shows that the swim pressure changes its scaling behavior from quadratic increase in gaseous phase to a power law increase with an exponent $3/2$ in phase-separated state. More importantly, the behavior of the swim pressure and effective diffusion coefficient is qualitatively related in the phase separated state with variation according to $Pe^{3/2}$ [18] and parabolic increase in the homogeneous phase.

The living crystals have been found in the study of various artificial swimmers driven by the interplay of various complex mechanisms [20, 21, 57]. Our study suggests that if the active colloid can sense the presence of neighboring colloids by reducing their speed, the aggregates can form at much smaller density. Although the mechanism behind self-propulsion and growth of such living colloids may vary in various systems, the physics behind the stability of such crystals is generic. Our study reveals the detailed analysis of various local forces behind the stability of such active crystals. The effect of viscous

lubrication, hydrodynamics, and anisotropic effect on the swimmers are excluded in our approach, which may be worthy to be taken into account for the study with more realistic approach.

V. ACKNOWLEDGEMENTS

All the computer simulations are performed on the HPC facility at IISER Bhopal. SPS acknowledges DST SERB Grant No. YSS/2015/000230 for financial support, SKA and FJ would like to thank Harsh Kumar for useful discussions at the initial stage of the work.

-
- [1] M. C. Marchetti, J.-F. Joanny, S. Ramaswamy, T. B. Liverpool, J. Prost, M. Rao, and R. A. Simha, *Reviews of Modern Physics* **85**, 1143 (2013).
- [2] M. E. Cates, *Reports on Progress in Physics* **75**, 042601 (2012).
- [3] A. Zöttl and H. Stark, *Journal of Physics: Condensed Matter* **28**, 253001 (2016).
- [4] L. Corte, P. M. Chaikin, J. P. Gollub, and D. J. Pine, *Nature Physics* **4**, 420 (2008).
- [5] F. Peruani, A. Deutsch, and M. Bär, *Physical Review E* **74**, 030904 (2006).
- [6] A. Gopinath, M. F. Hagan, M. C. Marchetti, and A. Baskaran, *Physical Review E* **85**, 061903 (2012).
- [7] O. Pohl and H. Stark, *Physical review letters* **112**, 238303 (2014).
- [8] Z. Lin, C. Gao, M. Chen, X. Lin, and Q. He, *Current opinion in colloid & interface science* **35**, 51 (2018).
- [9] V. Narayan, S. Ramaswamy, and N. Menon, *Science* **317**, 105 (2007).
- [10] H. Chaté, F. Ginelli, and R. Montagne, *Phys. Rev. Lett.* **96**, 180602 (2006).
- [11] G. S. Redner, A. Baskaran, and M. F. Hagan, *Phys. Rev. E* **88**, 012305 (2013).
- [12] T. Mora, A. M. Walczak, L. Del Castello, F. Ginelli, S. Melillo, L. Parisi, M. Viale, A. Cavagna, and I. Giardina, *Nature physics* **12**, 1153 (2016).
- [13] M. Ballerini, N. Cabibbo, R. Candelier, A. Cavagna, E. Cisbani, I. Giardina, V. Lecomte, A. Orlandi, G. Parisi, A. Procaccini, *et al.*, *Proceedings of the national academy of sciences* **105**, 1232 (2008).
- [14] A. Cavagna, D. Conti, C. Creato, L. Del Castello, I. Giardina, T. S. Grigera, S. Melillo, L. Parisi, and M. Viale, *Nature Physics* **13**, 914 (2017).
- [15] A. Bricard, J.-B. Caussin, D. Das, C. Savoie, V. Chikkadi, K. Shitara, O. Chepizhko, F. Peruani, D. Saintillan, and D. Bartolo, *Nature communications* **6**, 1 (2015).
- [16] J. Yan, M. Han, J. Zhang, C. Xu, E. Luijten, and S. Granick, *Nature materials* **15**, 1095 (2016).
- [17] Y. Fily and M. C. Marchetti, *Physical review letters* **108**, 235702 (2012).
- [18] R. G. Winkler, A. Wysocki, and G. Gompper, *Soft matter* **11**, 6680 (2015).
- [19] A. P. Solon, J. Stenhammar, R. Wittkowski, M. Kardar, Y. Kafri, M. E. Cates, and J. Tailleur, *Phys. Rev. Lett.* **114**, 198301 (2015).
- [20] J. Palacci, S. Sacanna, A. P. Steinberg, D. J. Pine, and P. M. Chaikin, *Science* **339**, 936 (2013).
- [21] D. P. Singh, U. Choudhury, P. Fischer, and A. G. Mark, *Advanced Materials* **29**, 1701328 (2017).
- [22] I. Buttinoni, J. Bialké, F. Kümmel, H. Löwen, C. Bechinger, and T. Speck, *Physical review letters* **110**, 238301 (2013).
- [23] I. Buttinoni, G. Volpe, F. Kümmel, G. Volpe, and C. Bechinger, *Journal of Physics: Condensed Matter* **24**, 284129 (2012).
- [24] F. Ginot, I. Theurkauff, F. Detcheverry, C. Ybert, and C. Cottin-Bizonne, *Nature communications* **9**, 696 (2018).
- [25] I. Theurkauff, C. Cottin-Bizonne, J. Palacci, C. Ybert, and L. Bocquet, *Physical review letters* **108**, 268303 (2012).
- [26] J. Palacci, S. Sacanna, S.-H. Kim, G.-R. Yi, D. Pine, and P. Chaikin, *Philosophical Transactions of the Royal Society A: Mathematical, Physical and Engineering Sciences* **372**, 20130372 (2014).
- [27] F. Schmidt, B. Liebchen, H. Löwen, and G. Volpe, *The Journal of chemical physics* **150**, 094905 (2019).
- [28] T. Vicsek, A. Czirók, E. Ben-Jacob, I. Cohen, and O. Shochet, *Physical review letters* **75**, 1226 (1995).
- [29] J. Toner and Y. Tu, *Physical review letters* **75**, 4326 (1995).
- [30] T. Vicsek and A. Zafeiris, *Physics reports* **517**, 71 (2012).
- [31] H. Chaté, F. Ginelli, G. Grégoire, F. Peruani, and F. Raynaud, *The European Physical Journal B* **64**, 451 (2008).
- [32] J. Toner, *Physical Review E* **86**, 031918 (2012).
- [33] G. S. Redner, M. F. Hagan, and A. Baskaran, *Physical review letters* **110**, 055701 (2013).
- [34] J. Bialké, T. Speck, and H. Löwen, *Journal of Non-Crystalline Solids* **407**, 367 (2015).
- [35] M. E. Cates and J. Tailleur, *Annu. Rev. Condens. Matter Phys.* **6**, 219 (2015).
- [36] M. E. Cates and J. Tailleur, *EPL (Europhysics Letters)* **101**, 20010 (2013).
- [37] P. Digregorio, D. Levis, A. Suma, L. F. Cugliandolo, G. Gonnella, and I. Pagonabarraga, *Physical review letters* **121**, 098003 (2018).
- [38] G. Gonnella, D. Marenduzzo, A. Suma, and A. Tiribocchi, *Comptes Rendus Physique* **16**, 316 (2015).
- [39] J. Barré, R. Chétrite, M. Muratori, and F. Peruani, *Journal of Statistical Physics* **158**, 589 (2015).
- [40] A. Suma, G. Gonnella, D. Marenduzzo, and E. Orlandini, *EPL (Europhysics Letters)* **108**, 56004 (2014).
- [41] E. Sese-Sansa, I. Pagonabarraga, and D. Levis, *EPL (Europhysics Letters)* **124**, 30004 (2018).
- [42] M. E. Cates and J. Tailleur, *EPL (Europhysics Letters)* **101**, 20010 (2013).
- [43] P. Digregorio, D. Levis, A. Suma, L. F. Cugliandolo, G. Gonnella, and I. Pagonabarraga, *Phys. Rev. Lett.* **121**, 098003 (2018).
- [44] L. Caprini, U. M. B. Marconi, and A. Puglisi, *Physical Review Letters* **124**, 078001 (2020).

- [45] B. Mahault, X.-c. Jiang, E. Bertin, Y.-q. Ma, A. Patelli, X.-q. Shi, and H. Chaté, *Physical review letters* **120**, 258002 (2018).
- [46] G. Grégoire and H. Chaté, *Physical review letters* **92**, 025702 (2004).
- [47] A. P. Solon, H. Chaté, and J. Tailleur, *Physical review letters* **114**, 068101 (2015).
- [48] J.-B. Caussin, A. Solon, A. Peshkov, H. Chaté, T. Dauxois, J. Tailleur, V. Vitelli, and D. Bartolo, *Physical review letters* **112**, 148102 (2014).
- [49] I. S. Aranson and L. S. Tsimring, *Physical Review E* **67**, 021305 (2003).
- [50] F. Ginelli, F. Peruani, M. Bär, and H. Chaté, *Physical review letters* **104**, 184502 (2010).
- [51] J. Deseigne, O. Dauchot, and H. Chaté, *Physical review letters* **105**, 098001 (2010).
- [52] A. Patch, D. Yllanes, and M. C. Marchetti, *Physical Review E* **95**, 012601 (2017).
- [53] S. P. Brown and R. A. Johnstone, *Proceedings of the Royal Society of London. Series B: Biological Sciences* **268**, 961 (2001).
- [54] B. J. Crespi, *Trends in ecology & evolution* **16**, 178 (2001).
- [55] C. Lupp and E. G. Ruby, *Journal of bacteriology* **187**, 3620 (2005).
- [56] V. Sperandio, A. G. Torres, and J. B. Kaper, *Molecular microbiology* **43**, 809 (2002).
- [57] T. Bäuerle, A. Fischer, T. Speck, and C. Bechinger, *Nature communications* **9** (2018).
- [58] S. R. McCandlish, A. Baskaran, and M. F. Hagan, *Soft Matter* **8**, 2527 (2012).
- [59] C. A. Velasco, M. Abkenar, G. Gompper, and T. Auth, *Physical Review E* **98**, 022605 (2018).
- [60] F. Farrell, M. Marchetti, D. Marenduzzo, and J. Tailleur, *Physical review letters* **108**, 248101 (2012).
- [61] M. Lee, K. Szuttor, and C. Holm, *The Journal of chemical physics* **150**, 174111 (2019).
- [62] H. C. Berg and D. A. Brown, *Nature* **239**, 500 (1972).
- [63] L. Turner, W. S. Ryu, and H. C. Berg, *Journal of bacteriology* **182**, 2793 (2000).
- [64] G. Ariel, M. Sidortsov, S. D. Ryan, S. Heidenreich, M. Bär, and A. Be'er, *Physical Review E* **98**, 032415 (2018).
- [65] J. Bialké, T. Speck, and H. Löwen, *Physical review letters* **108**, 168301 (2012).
- [66] T. Speck, J. Bialké, A. M. Menzel, and H. Löwen, *Physical Review Letters* **112**, 218304 (2014).
- [67] T. Speck, A. M. Menzel, J. Bialké, and H. Löwen, *The Journal of chemical physics* **142**, 224109 (2015).
- [68] J. Bialké, H. Lwen, and T. Speck, *EPL (Europhysics Letters)* **103**, 30008 (2013).
- [69] M. Pu, H. Jiang, and Z. Hou, *Soft Matter* **13**, 4112 (2017).
- [70] M. E. Cates, D. Marenduzzo, I. Pagonabarraga, and J. Tailleur, *Proceedings of the National Academy of Sciences* **107**, 11715 (2010).
- [71] S. K. Anand and S. P. Singh, *Physical Review E* **98**, 042501 (2018).
- [72] S. K. Anand and S. P. Singh, *Physical Review E* **101**, 030501 (2020).
- [73] J. Agudo-Canalejo and R. Golestanian, *Physical review letters* **123**, 018101 (2019).
- [74] M. Theers, E. Westphal, K. Qi, R. G. Winkler, and G. Gompper, *Soft matter* **14**, 8590 (2018).
- [75] A. Zöttl and H. Stark, *Physical review letters* **112**, 118101 (2014).
- [76] P. J. Steinhardt, D. R. Nelson, and M. Ronchetti, *Physical Review B* **28**, 784 (1983).
- [77] C. Tung, J. Harder, C. Valeriani, and A. Cacciuto, *Soft Matter* **12**, 555 (2016).